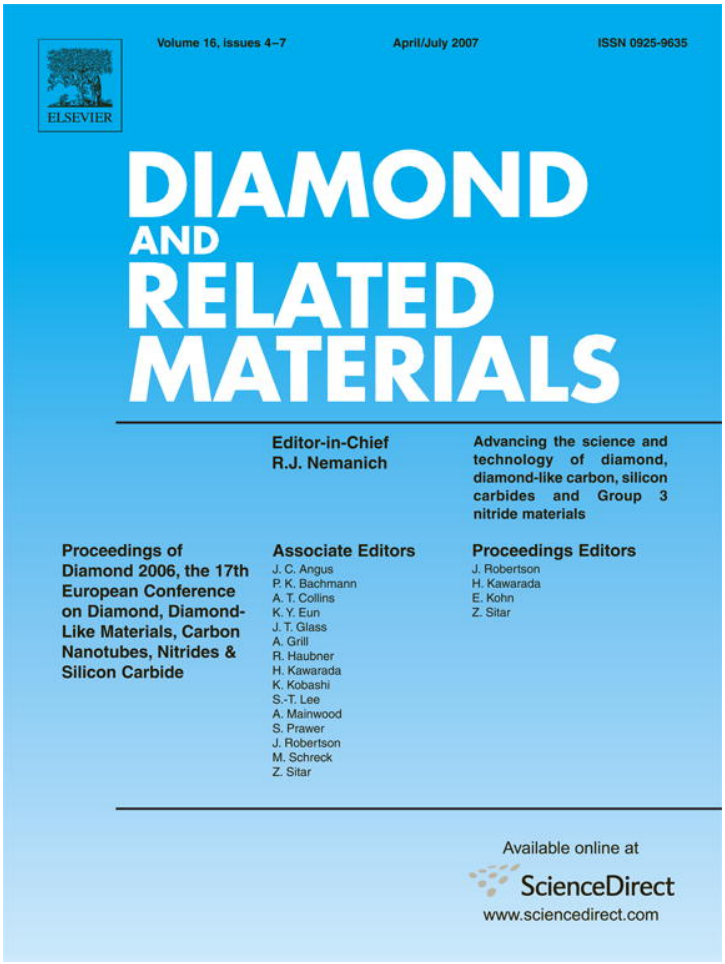

Available online at www.sciencedirect.com
ScienceDirect
Diamond & Related Materials 16 (2007) 690–694
DIAMOND AND RELATED MATERIALS
www.elsevier.com/locate/diamond

In situ study of the initial stages of diamond deposition on 3C–SiC (100) surfaces: Towards the mechanisms of diamond nucleation

J.C. Arnault [a,*,1], S. Saada [b], S. Delclos [b], L. Intiso [a,2], N. Tranchant [b], R. Polini [c], Ph. Bergonzo [b]

[a] CEA DSM-DRECAM-SPCSI, 91191 Gif sur Yvette, France
[b] CEA DRT-LIST-DETECS, 91191 Gif sur Yvette, France
[c] Dipertimento di Scienze e Tecnologie Chimiche, Università di Roma "Tor Vergata", Via della Ricerca Scientifica, 00133 Rome, Italy

Available online 4 January 2007

Abstract

The mechanisms involved in the diamond nucleation on 3C–SiC surfaces have been investigated using a sequential in situ approach using electron spectroscopies (XPS, XAES and ELS). Moreover, diamond crystals have been studied by HRSEM. The in situ nucleation treatment allows a high diamond nucleation density close to 4×10^{10} cm^{-2}. During the in situ enhanced nucleation treatment under plasma, a negative bias was applied to the sample. The formation of an amorphous carbon phase and the roughening of the 3C–SiC surface have been observed. The part of these competing mechanisms in diamond nucleation is discussed.

Keywords: Diamond crystal; Nucleation; Silicon carbide; Surface characterisation

1. Introduction

The intrinsic reactivity of a heterosubstrate under a Chemical Vapour Deposition (CVD) plasma strongly determines the mechanisms competing with diamond nucleation. These mechanisms have often detrimental consequences on the quality of the interface with diamond. Up to now, the mechanisms occurring during the diamond nucleation on 3C–SiC surfaces have been seldom studied [1,2]. Recently, the behaviour of different reconstructed 3C–SiC (100) surfaces after Microwave Plasma (MPCVD) exposure has been investigated [3,4]. Encouraging progress has been made towards highly oriented diamond film preparation on 3C–SiC surfaces [5]. The present study focuses on the mechanisms taking place at the SiC surface during a process including two successive steps in a MPCVD reactor. The first one is a necessary transition step to reach steady state conditions with stabilized plasma parameters. The second step is an in situ enhanced nucleation treatment under plasma using similar parameters except that, in this case, a negative bias voltage was applied to the substrate. The reactor is connected to a UHV analysis chamber allowing an in situ surface diagnostic via electron spectroscopies: X-ray Photoelectron Spectroscopy (XPS), X-ray Auger Electron Spectroscopy (XAES) and Energy Loss Spectroscopy (ELS). In order to investigate the nucleation mechanisms, a sequential approach was chosen with two different nucleation treatments.

2. Experimental

Single domain n-type 3C–SiC thin films (3 μm thick) epitaxially grown on a Si (100) substrate (3° off axis) were used. The sample size was about 1×1 cm^2. Plasma treatments were performed in the home designed MPCVD reactor, equipped with a 2.45 GHz–2 kW SAIREM microwave generator. The base pressure inside the chamber was about 10^{-9} mbar. The sample holder was placed on a molybdenum disk to minimize residual contamination from the support during the plasma discharge. High purity research grade gases were used: N55 for methane and N90 for hydrogen (with a catalytic purifier added to the gas line). First, surfaces have been exposed to a H_2/CH_4 (3%) mixture for 10 min to stabilize the plasma parameters and the substrate temperature. Then the in situ enhanced nucleation treatment under plasma was carried out. A negative bias voltage was applied to the substrate inducing an ion bombardment of

* Corresponding author. CEA Saclay DSM/DRECAM/SPCSI, 91191 Gif sur Yvette, France. Tel.: +33 1 69 08 71 02; fax: +33 1 69 08 84 46.
E-mail address: jean-charles.arnault@cea.fr (J.C. Arnault).
[1] On leave from: Université Louis Pasteur, Strasbourg, France.
[2] On leave from: Università di Roma Tor Vergata, Rome, Italy.

0925-9635/$ - see front matter © 2007 Elsevier B.V. All rights reserved.
doi:10.1016/j.diamond.2006.12.036

the surface. The bias voltage was tuned in order to enable full coverage of the secondary plasma on the substrate surface. During both steps, the gas pressure was 25 mbar and the microwave power 500 W. Sample 1 underwent the first CVD step only while two different in situ enhanced nucleation steps using two different bias voltages, −90 V and −180 V, were applied to samples 2 and 3, respectively. The duration of nucleation treatment was 10 min in both cases. During the nucleation step, the substrate temperature, as measured by a laser pyrometer, was maintained constant to 780 °C independent of the plasma parameters using a temperature-controlled substrate holder. Immediately after, the reactor was pumped to UHV pressures for transfer into the analysis chamber for surface analyses: XPS, XAES and ELS. XPS and XAES are complementary techniques because their penetration depths are very different: inelastic mean free paths for Si 2p and C 1s core levels are 3.2 nm and 3 nm, respectively [6] whereas Auger Si LVV and C KVV transitions probe a depth of 0.8 nm [7]. The XPS measurements were performed with a monochromatic Al Kα source. The same XPS conditions have been used for all the spectra. Curve fitting procedure was performed to extract the components in the C 1s and Si 2p spectra. Voigt functions were used with Lorentzian widths of 0.2 eV and 0.085 eV for C 1s and Si 2p core levels [8]. The Gaussian width was considered as an adjustable parameter. ELS spectra recorded at the carbon core level completed the identification of carbon phases. High Resolution Scanning Electron Microscopy (HRSEM) investigations were performed using a LEO Supra 35 equipped with a high brilliance Field Emission Gun ensuring a lateral resolution lower than 10 nm for our samples. The images were recorded in the Secondary Electron Image (SEI) mode using an acceleration voltage of 10 kV.

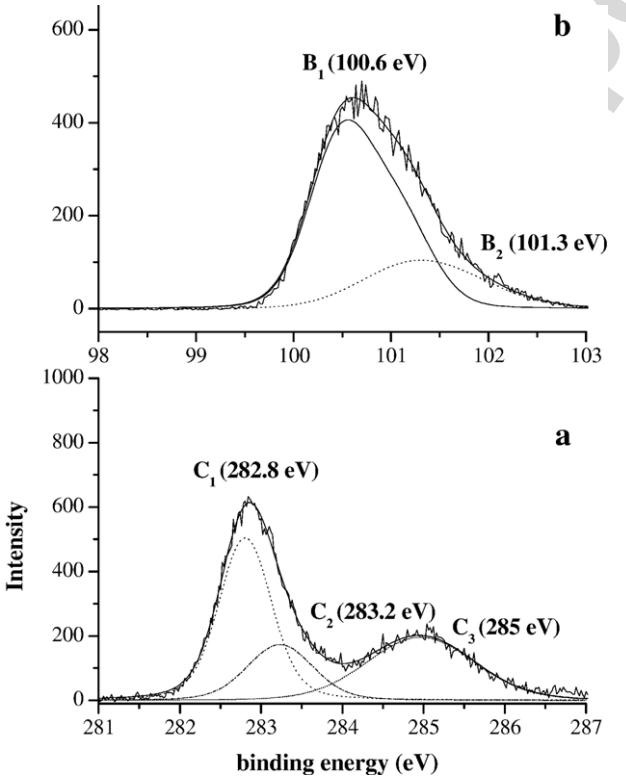

Fig. 1. XPS core level spectra of the 3C–SiC sample before any plasma treatment: a) C 1s core level; b) Si 2p core level. The components B_1, B_2, C_1, C_2 and C_3 are discussed in the text.

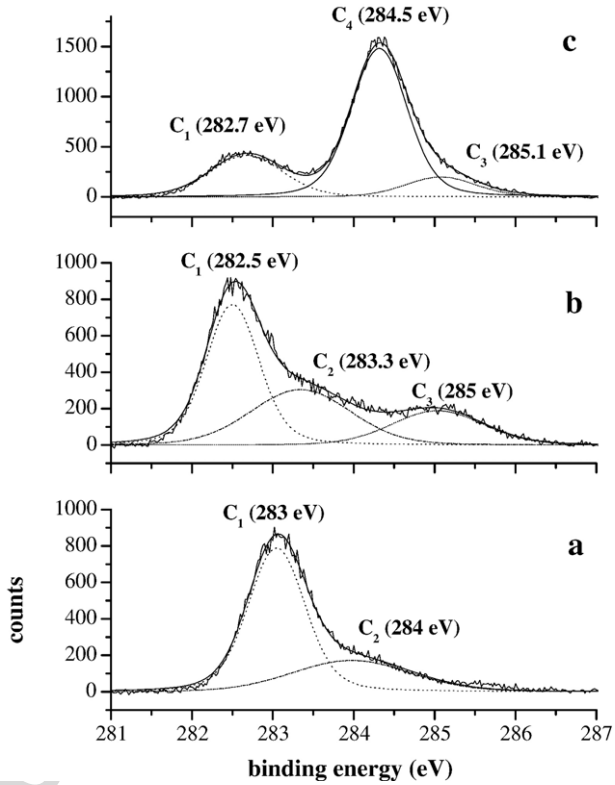

Fig. 2. C 1s XPS core level spectra of the three 3C–SiC (100) surfaces: a) sample 1: after the first CVD step; b) sample 2: after the first in situ enhanced nucleation step; c) sample 3: after the in situ enhanced nucleation step using a higher bias voltage. The components C_1, C_2, C_3 and C_4 are discussed in the text.

3. Results

This study has been carried out on as-introduced 3C–SiC samples. The XPS C 1s and Si 2p spectra before any plasma treatment are displayed in Fig. 1. At the carbon core level (Fig. 1a), the C_1 component located at 282.8 eV was attributed to bulk 3C–SiC lattice. Indeed, the energy difference with the 3C–SiC B_1 component at the Si 2p core level (Fig. 1b) was 182.2 eV close to the reported value [9]. A second component B_2 located at +0.7 eV was observed at the Si 2p core level. Moreover, a O 1s peak was detected. The B_2 component can be assigned to the formation of oxicarbides at the surface [10]. At the carbon core level, the C_3 component located at +2.2 eV with respect to C_1 could correspond to the Si–O–C bonds according to the literature [11]. Both B_2 and C_3 components are removed after the first CVD step (Figs. 2a and 3a). Another component C_2 at +0.4 eV is observed at the C 1s core level, and its assignation will be discussed below.

After the first CVD step, i.e. the plasma exposure preceding the enhanced nucleation treatment, only two components were observed at the C 1s core level for sample 1 (Fig. 2a). The main one C_1 at 283 eV is assigned to the carbon atoms belonging to

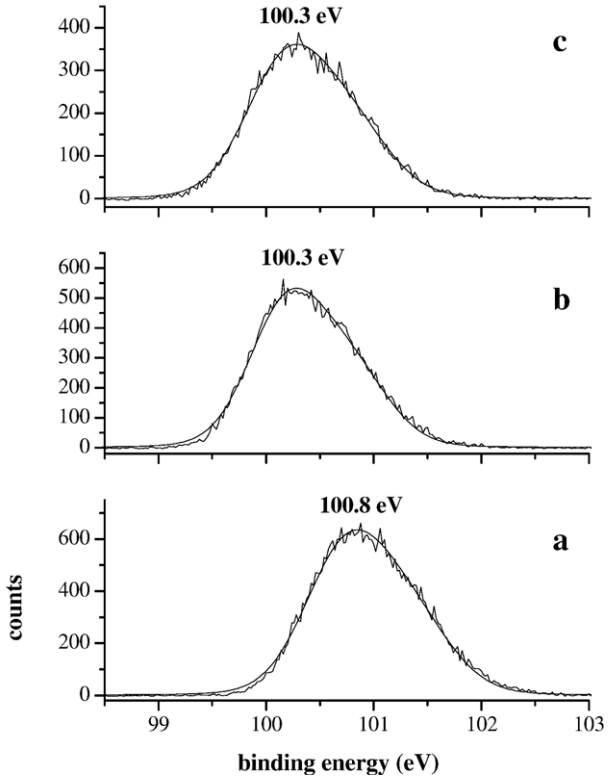

Fig. 3. Si 2p XPS core level spectra of the three 3C–SiC (100) surfaces: a) sample 1: after the first CVD step; b) sample 2: after the first in situ enhanced nucleation step; c) sample 3: after the in situ enhanced nucleation step using a higher bias voltage.

the 3C–SiC bulk lattice. The second one C_2 located at 284 eV is related to carbon atoms lying at the 3C–SiC surface [4]. The XAES C KVV/Si LVV ratio was close to 1.1, i.e. comparable to that of the c(2×2) reconstructed C-terminated surface [3] thus suggesting a carbon termination of the surface of the unreconstructed sample after plasma exposure. Nevertheless, a ~0.5 eV shift towards higher binding energy was observed for both C 1s components. The Si 2p core level which shows a unique component corresponding to the bulk 3C–SiC, exhibits a similar shift towards higher binding energy (Fig. 3a). The energy difference between B_1 and C_1 3C–SiC bulk components remained close to the reference value [9]. At the same time, XPS revealed the presence of oxygen at the surface after the CVD exposure, the XPS C 1s/O 1s area ratio is 5.7. This value is close to the one previously measured on C-terminated surfaces after comparable plasma treatment [4]. The binding energy shift disappeared as the oxygen was desorbed after annealing at 1050 °C (not shown). However, no additional component related to chemical bonding between oxygen and silicon was observed at the Si 2p core level (Fig. 3a). This effect is mostly related to physisorbed oxygen formed during the sample cooling when the plasma discharge was stopped.

Sample 2 underwent a first in situ enhanced nucleation step using a bias voltage of 90 V. The previous binding energy shift was no more observed at both C 1s and Si 2p core levels (Figs. 2b and 3b) because the oxygen amount was significantly lower. The C 1s core level was modified with the appearance of a new component C_3 located at 285 eV (Fig. 2b). This component has been systematically observed whatever the parameters of the enhanced nucleation step on 3C–SiC surfaces. For sample 2, the area of the C_3 component represented 19% of the total C 1s signal. The C_3 component could not be associated with graphite formation because it was located at +0.6 eV from the value obtained on a Highly Oriented Pyrolitic Graphite (HOPG) reference using the same XPS conditions. Moreover, no graphite characteristic structures such as the intense π–π* at 6.8 eV and the bulk plasmon at 27 eV were found in the corresponding ELS spectrum (Fig. 4b). Indeed, in addition to the bulk SiC plasmon A_1 at 22.5 eV [12], the ELS spectrum recorded at the C 1s core level showed a weak peak A_2 located at +7.5 eV from the C_3 component (Fig. 4b). This energy position of A_2 and the presence of the C_3 component at 285 eV are in agreement with the formation of a mixed sp^2/sp^3 carbon phase at the surface [13]. Moreover, the in situ enhanced nucleation step led to a subsequent carbon enrichment of the SiC surface in comparison with the previous surface stoichiometry. The XAES C KVV/Si LVV ratio was equal to 2.9 instead of 1.1 for sample 1. Nevertheless, diamond signal was detected neither at the C 1s core level nor in the ELS spectrum.

A second nucleation step was applied to sample 3 using a higher bias voltage, 180 V. As a consequence, the amount of carbon at and near the surface increased and the XAES C KVV/Si LVV ratio rose from 2.9 to 4.1. The predominant peak at the C 1s core level was a fourth component C_4 located at 284.5 eV (Fig. 2c). This BE position is in line with the diamond reference measured using the same experimental conditions. Its area represented 66% of the total C 1s intensity. The C_3 component previously assigned to amorphous carbon was always visible (11% of the total C 1s area). The diamond formation was further confirmed by the ELS spectrum (Fig. 4c) which exhibited the characteristic diamond bulk plasmon (A_3) at +34 eV from the C_4 component [14]. The A_3 peak was well comparable to our

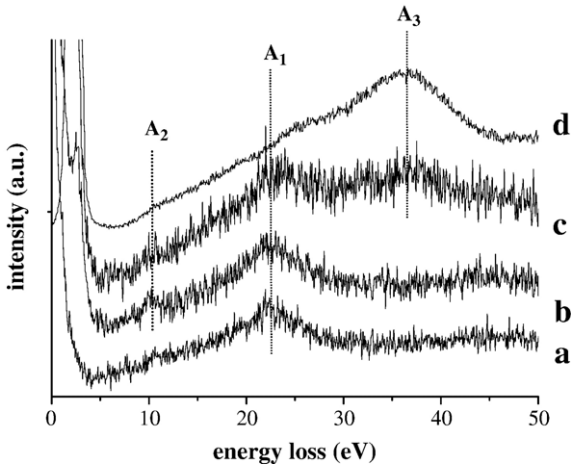

Fig. 4. ELS spectra recorded at the C 1s core level, the zero of energy corresponds to the bulk 3C–SiC C_1 peak: a) sample 1: after the first CVD step; b) sample 2: after the first in situ enhanced nucleation step; c) sample 3: after the in situ enhanced nucleation step using a higher bias voltage; d) diamond reference studied using the same experimental conditions. The structures A_1, A_2 and A_3 are discussed in the text.

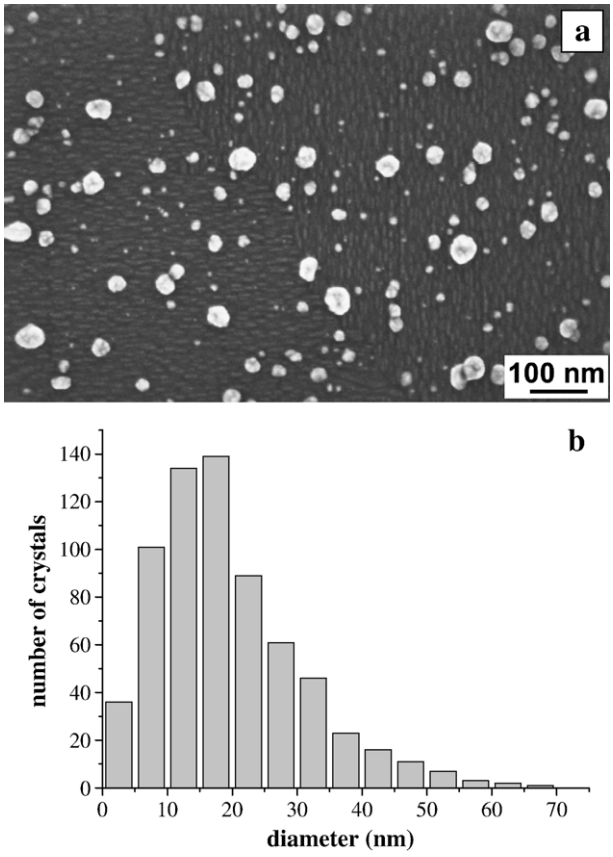

Fig. 5. a) High resolution SEM picture of diamond crystallites nucleated at the surface of sample 3. Anisotropic stripes are visible on the substrate areas not covered by diamond. b) Corresponding size distribution function of diamond crystallites.

internal diamond reference (Fig. 4d), showing a similar shape in the 10–30 eV range, except the remaining SiC bulk plasmon A_1 (Fig. 4c). The Si 2p unique peak is located at the same binding energy compared to the first nucleation treatment (Fig. 3b–c). The higher carbon amount at the surface leads to the attenuation of its intensity. HRSEM investigations have been performed to characterize the distribution of diamond crystals. A typical picture is shown in Fig. 5a. The nucleation density calculated over several tens of images was 4.10^{10} cm^{-2}. Image analysis of SEM pictures showed that the surface covered by diamond crystals was 13% of the total surface. The size distribution function of diamond crystals was calculated considering 700 particles and is displayed in Fig. 5b. The mean equivalent diameter ($d=(4A/\pi)^{1/2}$ where A is the projected area of each particle) was around 20 nm and the FWHM value was 20 nm. The high resolution SEM pictures exhibited stripes elongated in perpendicular directions (anisotropic stripes, according to Ref. [2]). These stripes represent two equivalent domains of different phases in 3C–SiC [15] and were detectable only in those samples that gave large nucleation density values under suitable in situ enhanced nucleation treatments (Fig. 5a). Between the crystals, the standard deviation of the height values measured by AFM (RMS roughness) was close to 0.9 nm while it was 0.3 nm for sample 1 which underwent the first plasma exposure step only. Therefore, the in situ nucleation treatment induced a significant surface roughening.

4. Discussion and summary

After the H_2/CH_4 (3%) exposure that allows the surface to reach steady state conditions, the surface stoichiometry of the 3C–SiC (100) sample corresponds to that typical of carbon-terminated surfaces. The C-termination hypothesis is well supported by both the C_2 component observed at the C 1s core level at +1 eV versus the C_1 bulk peak and the XAES C KVV/Si LVV ratio. The in situ enhanced nucleation treatment under plasma starts on a carbon-terminated 3C–SiC surface. The in situ enhanced nucleation step has three main consequences at the 3C–SiC surface. First, when an intense plasma sheath is used (sample 3), a very high diamond nucleation density close to 4×10^{10} cm^{-2} is obtained. Second, an amorphous carbon phase that could not be detected after the preceding plasma stabilization step (Fig. 2a), was formed. On the other hand, the formation of amorphous carbon has been observed whatever the parameters governing the enhanced in situ nucleation treatment and independent of the diamond density. Third, the in situ nucleation step led to a rougher silicon carbide surface as revealed by the RMS roughness measured by AFM (0.9 nm instead of 0.3 nm). High resolution SEM pictures showed the presence of typical anisotropic stripes at the SiC surface not covered by diamond (Fig. 5a). It is worth noting that these stripes (or protrusions) could not be detected by SEM in samples 1 and 2, where diamond nucleation was practically nil. This fact suggests that the anisotropic stripes, elongated along the <110> directions and formerly observed after bias enhanced nucleation (BEN) treatment [2,15], might form only under those conditions that effectively lead to a huge enhancement of diamond nucleation on SiC buffer layers.

Sueseda et al. [2] hypothesized that the formation of the stripe structure could be due to either deposition of SiC, where Si was supplied from the walls of their quartz reactor, or H_2 plasma etching. However, these mechanisms can not be invoked in our study because i) the surface stoichiometry, as determined by XAES, clearly demonstrated a carbon enrichment and ii) our previous experiments [4] showed that the etching by H_2 plasma is negligible for C-terminated 3C–SiC surfaces. Therefore, the formation of anisotropic stripes seems related to atomic surface diffusion processes activated by bombardment of ions with suitable kinetic energy.

The in situ enhanced nucleation step was able to produce a very high diamond nucleation density (4×10^{10} cm^{-2}) on 3C–SiC surfaces whose morphology was modified by the formation of the stripe structure and consequent surface roughening. Moreover, the nucleation step led also to the co-deposition of amorphous carbon whose role in the mechanism leading to diamond nucleation is still unclear at the present time. The literature clearly shows that amorphous carbon can be involved in the formation of diamond nuclei on silicon and iridium substrates but with different consequences. Recently, the nucleation and growth of oriented diamond crystals at the interface with iridium covered by a thin amorphous carbon layer

has been demonstrated [16]. In this case, the amorphous carbon has a protective role preserving diamond nuclei from the reactive species produced in the plasma. This allows the formation of oriented diamond domains at the iridium surface. For silicon, the formation of diamond nuclei within an amorphous carbon matrix was also underlined [17]. In contrast to iridium, most of the resulting diamond crystals are embedded in the amorphous carbon. Further experiments are under progress to investigate the role of both amorphous carbon and surface stoichiometry in the diamond nucleation on 3C–SiC surfaces.

Acknowledgement

Dr. R. Polini gratefully thanks CEA for supporting Miss Luciana Intiso during her stay at the *Département de Recherche sur l'État Condensé, les Atomes et le Molécules* (DRECAM).

References

[1] B.R. Stoner, J.T. Glass, Appl. Phys. Lett. 60 (1992) 698.
[2] T. Suesada, N. Nakamura, H. Nagasawa, H. Kawarada, Jpn. J. Appl. Phys. 34 (1995) 4898.
[3] M. Portail, S. Saada, S. Delclos, J.C. Arnault, P. Soukiassian, P. Bergonzo, T. Chassagne, A. Lescuras, Phys. Status Solidi, A Appl. Res. 202 (2005) 2234.
[4] J.C. Arnault, S. Delclos, S. Saada, N. Tranchant, Ph. Bergonzo, J. Appl. Phys. 101 (2007) 014904.
[5] Private communication, CEA DRT/LIST/DETECS/SSTM report-05/043.
[6] S. Tanuma, C.J. Powell, D.R. Penn, Surf. Interf. Anal. 11 (1988) 577.
[7] C.J. Powell, A. Jablonski, A. Naumkin, A. Kraut-Vass, J.M. Conny, J.R. Rumble Jr., J. Electron Spectrosc. Relat. Phenom. 114–116 (2001) 1097.
[8] M.G. Silly, J. Roy, H. Enriquez, P. Soukiassian, C. Crotti, S. Fontana, P. Perfetti, J. Vac. Sci. Technol., B 22 (2004) 2226.
[9] F.R. Mc Feely, S.P. Kowalczyk, L. Ley, R.G. Cavell, R.A. Pollack, D.A. Shirley, Phys. Rev., B 9 (1974) 5268.
[10] Y. Hijikata, H. Yaguchi, M. Yoshikawa, S. Yoshida, Appl. Surf. Sci. 184 (2001) 161.
[11] G.D. Soraru, G. D'andrea, A. Glisenti, Mater. Lett. 27 (1996) 1.
[12] R.J. Meilunas, R.P.H. Chang, S. Liu, M.M. Kappes, Appl. Phys. Lett. 59 (1991) 3461.
[13] S. Rey, F. Antoni, B. Prevot, E. Fogarassy, J.C. Arnault, J. Hommet, F. Le Normand, P. Boher, Appl. Phys., A 71 (2000) 433.
[14] Y. Wang, R.W. Hoffman, J.C. Angus, J. Vac. Sci. Technol., A, Vac. Surf. Films 8 (1990) 2226.
[15] H. Kawarada, T. Suesada, H. Nagasawa, Appl. Phys. Lett. 66 (1995) 583.
[16] M. Schreck, F. Hörmann, S. Gsell, Th. Bauer, B. Stritzker, Diamond Relat. Mater. 15 (2006) 460.
[17] Y. Lifshitz, X.M. Meng, S.T. Lee, R. Akhveldiany, A. Hoffman, Phys. Rev. Lett. 93 (2004) 056101.